Effect of Polymeric Stabilizers on Fischer-Tropsch Synthesis Catalyzed by Cobalt Nanoparticles supported on TiO_2

Jorge A. Delgado,[a] Carmen Claver,[a,b] Sergio Castillón,[c] Daniel Curulla-Ferré,[d] Vitaly V. Ordomsky,[e] and Cyril Godard[b]*

[a] Centre Tecnòlogic de la Química, 43007, Tarragona, Spain.

[b] Departament de Química Física i Inorgànica, Universitat Rovira I Virgili, C/ Marcel.li Domingo s/n, 43007 Tarragona, Spain. Fax: (+34) 977 559563; E-mail: cyril.godard@urv.cat

[c] Departament de Química Analítica i Orgànica, Universitat Rovira i Virgili, C/ Marcel.li Domingo s/n, 43007 Tarragona, Spain

[d] Total Research and Technology Feluy, Zone Industrielle Feluy C, B-7181 Seneffe, Belgium

[e] Unité de Catalyse et de Chimie du Solide, USTL-ENSCL-EC Lille, Bât. C3, Cite Scientifique, 59655 Villeneuve d'Ascq, France. Fax: (+33) 320 436 561.

Abstract

A series of colloidal cobalt nanoparticles of *ca.* 2.6 nm stabilized by several polymeric stabilizers were synthesized in water using sodium borohydride as reducing agent and subsequently immobilized on TiO_2. Both colloidal and TiO_2 supported NPs were characterized by TEM, HRTEM, XRD, XPS, TGA and ICP techniques and the catalytic performance of the supported NPs evaluated in the Fischer-Tropsch synthesis. Important differences in terms of activity were observed depending on the polymeric stabilizers used for the synthesis of the CoNPs. These differences were correlated with the catalyst reducibility, the presence of polymer stabilizer and boron and the reduction degree at the metal surface.

Keywords: Fischer-Tropsch synthesis, cobalt nanoparticles, polymeric stabilizers, sodium borohydride.

1 Introduction

Fischer-Tropsch Synthesis (FTS) is considered a key process of the XTL technologies (biomass-to-liquid, BTL, gas-to-liquid, GTL, and coal-to-liquid, CTL) since through this catalytic reaction, syngas (a mixture of H_2 and CO) can be transformed into clean fuels.[1-3] Among the metals active in FTS, there is a renewed interest in cobalt catalysts due to its higher activity and stability compared to iron.[4]

Currently, one of the main challenges in FT research is the design of not only active and stable catalysts but also highly selective active phases that provide hydrocarbons with narrow chain length distributions.[5] In this context, the advances in colloidal nanoscience have provided a more efficient control over the size and morphology of metallic nanoparticles with potential applications in the field of catalysis.[6] However, when colloidal NPs are used in catalysis, the effect of the stabilizing agent arises as an intrinsic characteristic for these catalysts. It is often considered that the activity of NPs tends to decrease with increasing coordination strength of the organic stabilizing agent to the metal surface,[7] as reported for hydrogenation,[8, 9] and C-C coupling reactions.[10] For instance, the possibility to tune the selectivity in the Ru- and RhNPs-catalyzed hydrogenation of aromatic ketones through the phosphorus stabilizing ligand has been recently reported in our research group.[8] For FTS, only a few studies involving RuNPs have been dedicated to the rationalization of the effect of the stabilizing agent.[7, 11] Hensen and co-workers reported the deposition of the organic stabilizing agents trimethyl(tetradecyl)ammonium bromide (TTAB), polyvinylpyrrolidone (PVP) and sodium 3-mercapto-1-propanesulfonate (SMPS) onto a previously prepared Ru/CNF (carbon nanofiber) catalyst with the aim to maintain the size and morphology of these particles. They observed that the activity in the FT reaction decreased in the order: Ru>Ru-TTAB>Ru-PVP>>Ru-SMPS and correlated this activity order with the interaction strength between the organic stabilizing agent and the Ru surface.[7] Using a different approach for the catalyst preparation, Chaudret and co-workers studied the reactivity of ligand-capped ruthenium nanocatalyst (PVP or diphosphine ligand) in model FTS reactions.[11] They reported that the surface modification by ligands, whether introduced as protecting agents during synthesis or afterward via ligand exchange, affected both selectivity and activity in catalysis, being more active those NPs stabilized by the diphosphine ligand with a higher selectivity towards light hydrocarbons (C_2-C_4) in comparison to the PVP-stabilized NPs. More recently, the same authors

Kou and co-workers tested RuNPs stabilized by PVP-K15, K30 and K90 (corresponding to polymers of molecular weights of 10000, 40000 and 36000, respectively) in the Aqueous phase Fischer-Tropsch Synthesis (AFTS).[12] A fast aggregation and deactivation of the catalysts prepared using the PVP-K15 was observed in catalysis. Interestingly, the activity of the catalyst prepared in the presence of the polymer of highest molecular weight, PVP-K90, was slightly lower than the stabilized by PVP-K30. It was proposed that the high coverage by PVP in the case of PVP-K90 may block the route for the reactants towards the metal surface, thus resulting in a lower catalytic activity.

In the case of cobalt, all the reports on FTS catalyzed by colloidal CoNPs involve the use of PVP or ionic liquids as stabilizers. Kou and co-workers reported several studies concerning the application of monometallic CoNPs,[13] and bimetallic Pt-Co NPs,[14] stabilized by PVP as catalysts of the AFTS. These authors also described the effect of the

reducing agent ($LiBEt_3H$ and $NaBH_4$) used for the preparation of CoNPs in the AFTS,[15] and proposed that doping by boron could affect the catalytic performance of these NPs. Very recently, Chaudret and co-workers reported the preparation of bimetallic Fe@FeCo and Fe@Ru NPs by thermal decomposition of $Co_2(CO)_8$ or $Ru_3(CO)_{12}$ carbonyls in the presence of preformed FeNPs.[16] Interestingly, the combination of magnetic and surface catalytic properties of these NPs was used to demonstrate the possibility of performing Fischer−Tropsch syntheses by heating the catalytic nanoparticles with an external alternating magnetic field.

Dupont and co-workers reported the synthesis of Co nanocubes (54 ± 22 nm)[17] and nanospheres (7.7 ± 1.2 nm)[18] by thermal decomposition of $Co_2(CO)_8$ in $[DMI][NTf_2]$ and $[BMI][NTf_2]$ respectively. In catalysis, a higher TOF in FTS was observed with the spheric CoNPs in comparison to the nanocubes (0.26 vs. $1.17x10^{-5}$ $mol_{CO}mol_{Suf\text{-}Co}^{-1}h^{-1}$). However, to the best of our knowledge, no reports on the effect of the stabilizing agent have been described to date for Co-catalyzed FTS.

In the present work, the effect of the polymer stabilizer on the catalytic performance of cobalt nanoparticles in FTS is rationalized. For this purpose, a series of small CoNPs was prepared by chemical reduction using sodium borohydride in the presence of several polymeric stabilizers and subsequently immobilized on TiO_2. This synthetic approach allowed the fine modulation of the cobalt particle size prior to their immobilization on the solid support, thus avoiding calcination treatments which often result in undesirable cobalt-support reactions.

2 Experimental

2.1. Materials and methods

All syntheses of CoNPs were carried under aerobic conditions using a mechanical stirrer. Milli-Q water was used for all the experiments. Solvents were purchased from Merck and used as received. $CoCl_2{\cdot}6H_2O$, $NaBH_4$ and the water soluble polymers were purchased from Sigma-Aldrich. Hydrogen (5.0) was purchased from Air Liquide and CO (4.7) and argon (5.0) from Carburos Metálicos.

Transmission electron microscopy (TEM) and high resolution transmission electron microscopy (HR-TEM) measurements were performed using a Zeiss 10 CA and a JEOL 2011(FEG) electron microscopes, respectively. X-ray diffraction (XRD) patterns were recorded on a Siemens D5000 diffractometer using Cu Kα radiation. Continuous scan mode was used to collect data over the 2θ range of 15° to 90°. X-ray Photoelectron Spectroscopy (XPS) data were obtained with a PHI 5500 Multitechnique System electron spectrometer from Physical Electronics using 350 W Al Kα radiation. The base pressure was about 2×10^{-8} torr. Fourier transform infrared (FT-IR) spectra were obtained as potassium bromide pellets with a resolution of 4 cm^{-1} and 32 scans in the range of 400–4000 cm^{-1} using a Bruker Equinox 55 spectrophotometer. Thermogravimetric analyses (TGA) were carried out on a Mettler

TGA/SDTA851e thermobalance. Samples (*ca.*0.01 g) were heated from room temperature up to 900 °C with 10 K min^{-1} under nitrogen flow using alumina holders. Elemental analysis of cobalt was performed by inductively coupled plasma-optical emission spectrometry (ICP-OES) using a Spectro Arcos FHS-16 spectrometer. Temperature programmed reduction under H_2 (TPR) was carried out using a ChemBET™ TPR/TPD (Quantachrome). The samples (*ca.* 0.1 g) were heated up to 900 ºC under 5% H_2/Ar flow (30 cm^3 min^{-1}) using alumina crisols. The temperature ramp was 10 ºC min^{-1}. BET areas were calculated from the nitrogen adsorption isotherms at -196 ºC using a Quadrasorb SI equipment. All the samples were degassed at 90 ºC during 24 h prior to the physisorption measurements.

2.2. Synthesis of colloidal cobalt nanoparticles by chemical reduction (Co1-6)

The CoNPs **Co1-Co6** were synthesized by chemical reduction of cobalt chloride in the presence of various water soluble polymeric stabilizers and using sodium borohydride as reducing agent. As a standard procedure, 0.226 g of $CoCl_2.6H_2O$ (0.931 mmol) was dissolved in H_2O containing the corresponding amount of the polymeric stabilizer (polymer:Co ratio varied from 1 to 40). The volume of water for all the syntheses was completed to 50 ml to obtain a cobalt concentration of 0.018 M. Then, a freshly prepared solution of 0.358 g of $NaBH_4$ (9.31 mmol) in 16.6 ml H_2O was added at room temperature with a rate of 3 ml/min (5 min). The solution was maintained under vigorous mechanical stirring for 2 h. Then 100 µl of the colloidal solution was centrifuged, washed with water and re-dispersed by sonication. Three drops of the obtained colloidal solution was deposited on a Cu-formvar or holey carbon grids for TEM or HR-TEM analysis. For the isolation of the CoNPs, the freshly prepared NPs were initially precipitated by a strong magnetic field and the supernatant was decanted. Then, the precipitated NPs were washed with water to remove the excess of salts and polymers. The decantation and washing process was repeated three times with water, ethanol and hexane. The resulted CoNPs were finally dried under vacuum and kept in the glove box. The size, the crystalline structure and oxidation state of the CoNPs were studied using transmission electron microscopy (TEM), HR-TEM, X-ray diffraction (XRD), and X-ray photoelectron spectroscopy (XPS) respectively. The composition of the CoNPs was studied using FTIR, TGA and ICP-OES.

2.3. Immobilization of cobalt nanoparticles on TiO_2 (Co1-6/TiO_2)

Isolated CoNPs (55 mg approximately) were re-suspended in 20 ml of hexane and sonicated during 3 minutes. Separately, a suspension of TiO_2 (0.490 g of 20 nm nanopowder, Degussa P25) in 40 ml of hexane was sonicated during 1 min and then mechanically stirred. The amount of TiO_2 was varied to obtain a 10 wt% Co catalyst. Then the suspension of CoNPs in hexane was added dropwise over the stirred suspension of TiO_2 and the resulting mixture stirred

during 30 min. The gray suspension was then sonicated during 3 min and the resultant solid was magnetically precipitated, the hexane removed and the solid dried under vacuum.

The obtained powders were pelletized, crushed and sieved to get grain sizes between the 0.300 - 0.150 mm prior to the catalytic tests.

2.4. Fischer-Tropsch catalytic experiments using the TiO_2 supported catalysts (Co1-6/TiO_2)

Fischer-Tropsch experiments using supported catalysts were carried out in a Flowrence high throughput unit[19] equipped with 16 parallel milli-fixed reactors (d_{int} = 2 mm) operating at a total pressure of 20 bar, H_2/CO = 2 molar ratio and GHSV = 6700 cm^3/g h. The catalyst loading in the micro-reactors was 100 mg. Prior to the catalytic test, all the samples were activated in a flow of pure hydrogen at atmospheric pressure during 10 h at 673 K with at GHSV = 2 NL h^{-1} g^{-1}. During the reduction, the temperature ramp was 1 K/min. After the activation, the catalysts were cooled down to 433 K and a flow of premixed syngas was gradually introduced through the catalysts. When pressure attained 20 bar, the temperature was slowly increased to 513 K with a ramp of 1 K/min. Gaseous reaction products were analyzed by on-line gas chromatography. Analysis of permanent gases was performed using a Molecular Sieve column and a thermal conductivity detector. Carbon dioxide and C_1–C_4 hydrocarbons were separated in a PPQ column and analyzed also by a thermal conductivity detector. C_5–C_{12} hydrocarbons were analyzed using CP-Sil5 column and a flame-ionization detector. The carbon monoxide contained 5% of helium, which was used as an internal standard for calculating carbon monoxide conversion. Catalytic rates and selectivities were measured at the steady-state regime after 46 h time-on-stream. The reaction rates expressed in cobalt time yield h^{-1}, are defined as the moles of CO converted per mol of Co per hour. The product selectivity (*S*) is reported as the wt% of a given product.

3. Results and Discussion

3.1. Synthesis and characterization of CoNPs Co1-Co6

The CoNPs **Co1-Co6** were synthesized in water by chemical reduction of cobalt chloride in the presence of polymeric stabilizers and using sodium borohydride as reducing agent. The structures of the water soluble polymers used to stabilize these CoNPs are displayed in Figure 1.

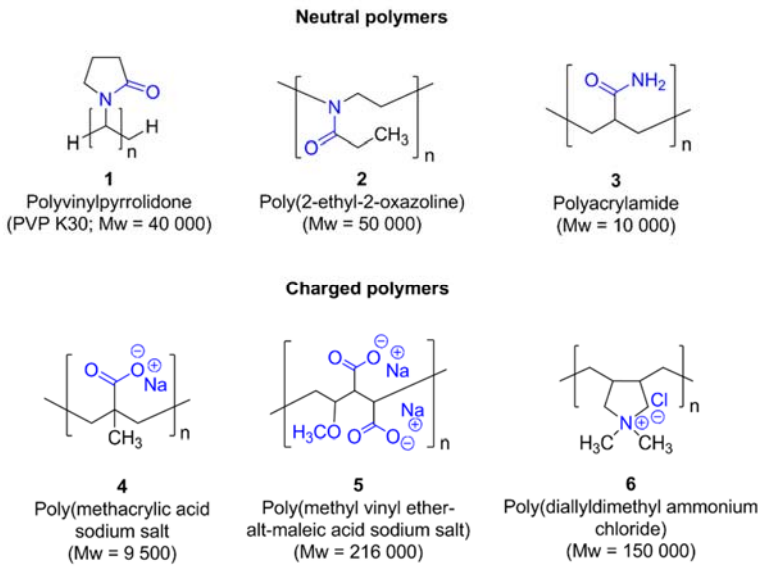


Figure 1. Structures of the water soluble polymers (**Polymers1-6**) used as stabilizers for CoNPs.

To prepare CoNPs of similar size for each one of the polymeric stabilizers, several sets of NPs were synthesized varying the polymer:Co ratio between 1 and 40 (Supporting Information). The variation of the stabilizer to metal ratio is a method widely applied for the control of the size of metal nanoparticles.[20-23] The TEM micrographs and size histograms of CoNPs **Co1-6** (stabilized by **Polymer1-6,** respectively) are displayed in Figure 2. CoNPs of *ca*. 2.6 nm were produced using a polymer:Co ratio of 20 for most of the polymeric stabilizers. Only in the case of **Polymer5**, NPs of such size were obtained using a polymer:Co ratio of 1 (**Co5**, 2.55 ± 0.49 nm). The small particle size observed for **Co5** at such a low polymer:metal ratio could be attributed to the relatively large molecular weight of this polymer (Mw = 216000), as previously reported for AuNPs.[24]

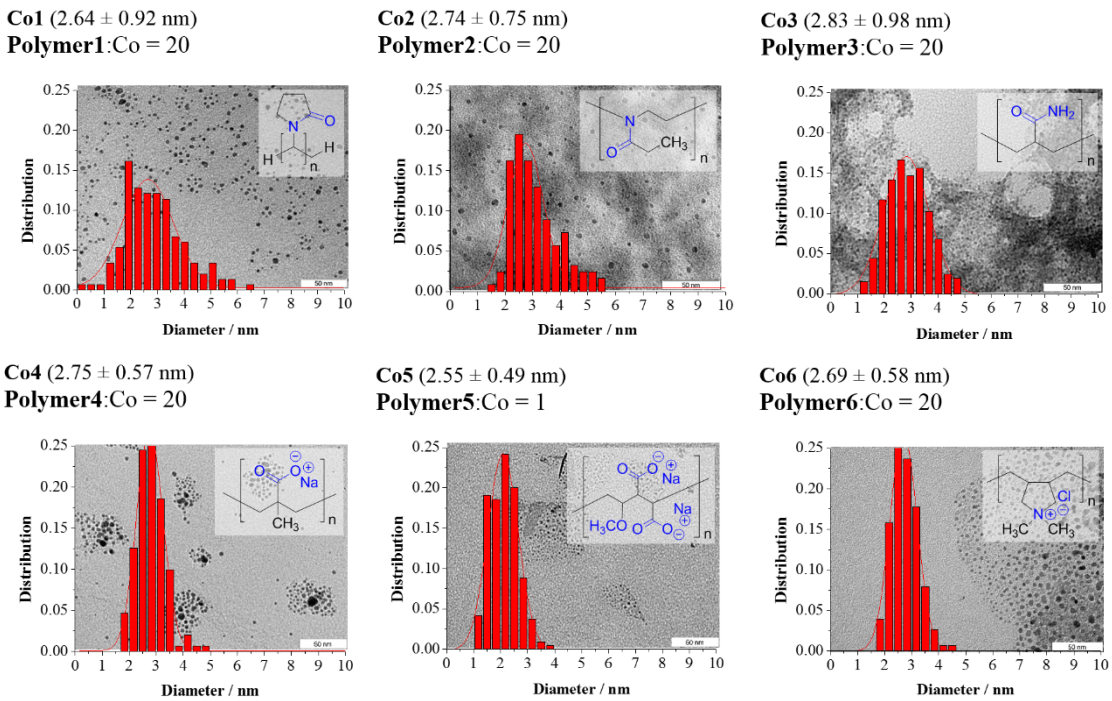


Figure 2. TEM micrographs and size histograms of **Co1-6** NPs.

The size and the fine structure of the CoNPs **Co1** and **Co5** were studied by high-resolution transmission electron microscopy (HR-TEM). In the micrograph of **Co1** displayed in Figure **3**, single particles of *ca.* 2-3 nm were observed in agreement with previous TEM observations (2.64 ± 0.92 nm).

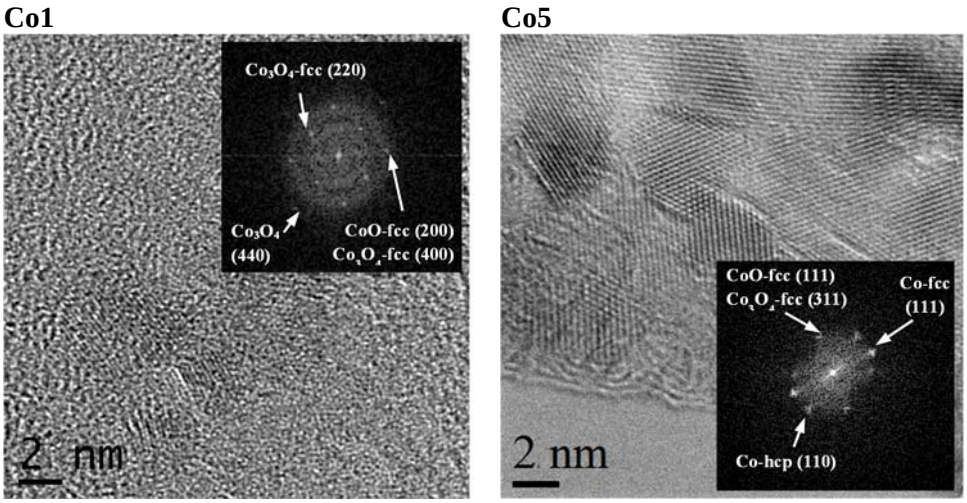


Figure 3. HR-TEM image of **Co1** and **Co5** NPs and their electron diffraction patterns.

Analysis of the electron diffraction pattern of **Co1** NPs revealed the presence of crystalline oxides, CoO-fcc/Co_3O_4-fcc, although no crystalline metallic cobalt phase was identified. In contrast, for **Co5,** the presence of both Co-fcc and CoO/Co_3O_4-fcc was observed. These differences suggest an influence of the polymer stabilizer on the fine structure of the resulting NPs. Possibly, the relatively large molecular weight of **Polymer5** could provide a higher steric hindrance resulting in a more ordered aggregation process.

Analysis of the crystalline structure of the catalysts **Co1-6** was performed by XRD (Supporting Information). The diffraction pattern of these materials revealed the presence of broad bands at *ca.* 45º, 35 and 60º which did not allow the unambiguous identification of either cobalt, cobalt oxide or boride phases. The broadening of XRD peaks (centered at 45º) was previously observed for CoNPs prepared by $NaBH_4$ reduction,[25, 26] and is frequently associated to the small size and/or to the amorphous structure of NPs.[27, 28]

In order to gain insights into the structure and composition of the CoNPs, the methodology reported by Glavee *et al*. consisting in the thermal treatment of the CoNPs under Ar atmosphere was applied.[29] Through this procedure, the CoNPs are forced to crystallize (or increase in size) thus revealing the crystalline pattern of their components. After such treatment, the presence of metallic cobalt phases (fcc and hcp) was evidenced for **Co1,2,5,6** (Figure 4). Moreover, the detection of a peak located at 28º was attributed to a boron species in the case of **Co1**. In contrast, **Co3** and **Co4**, exhibited a mixture of metallic cobalt of cobalt oxide phases (CoO-fcc). It was therefore concluded that the NPs **Co1-6**, were indeed constituted by metallic cobalt, although in the case of **Co3** and **Co4**, important amounts of cobalt oxide were also present. These observations suggest that the nature of the polymeric stabilizer used during the synthesis can affect the final composition of the resulting CoNPs.

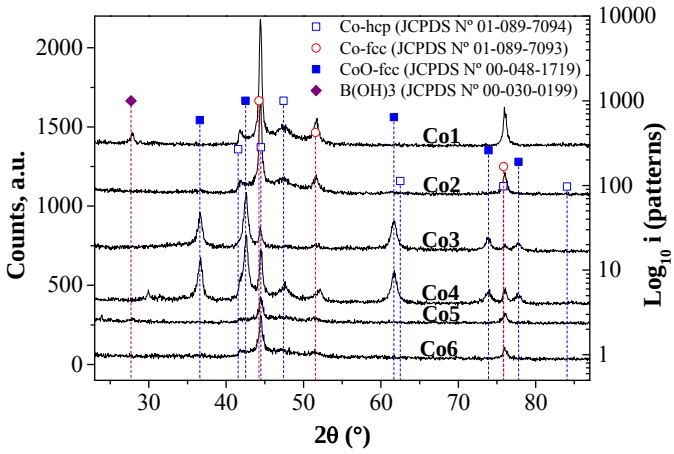


Figure 4. XRD patterns of **Co1-6** after treatment at 500 ºC under argon for 2 h.

Surface analysis of the CoNPs synthesized in this study was performed by X-ray photoelectron spectroscopy (XPS). The full XPS spectra of **Co1-6** revealed the presence of Na, Co, O, N, C and B, according to the peaks observed at their characteristic binding energies (1071.6; 781.5; 530.9; 399.2; 284.5 and 191.1 eV respectively). The Co 2p XPS spectra of the series **Co1-6** exhibited two main sets of peaks at *ca.* 777-794 and 795-806 eV that were readily assigned to Co $2p_{3/2}$ and Co $2p_{1/2}$, respectively (Figure 5). The fractions of Co^0 and Co^{2+} extracted from the decomposition of the Co $2p_{3/2}$ spin orbit peaks are displayed in Table 1.[30] A metallic cobalt content ranging from 6 to 67% was calculated for this series of NPs. **Co5** exhibited the highest content in metallic cobalt (67 %) while **Co2**, **Co3** and **Co4**, presented values of 25-30%. In the case of **Co6**, only 6% of Co^0 was determined.

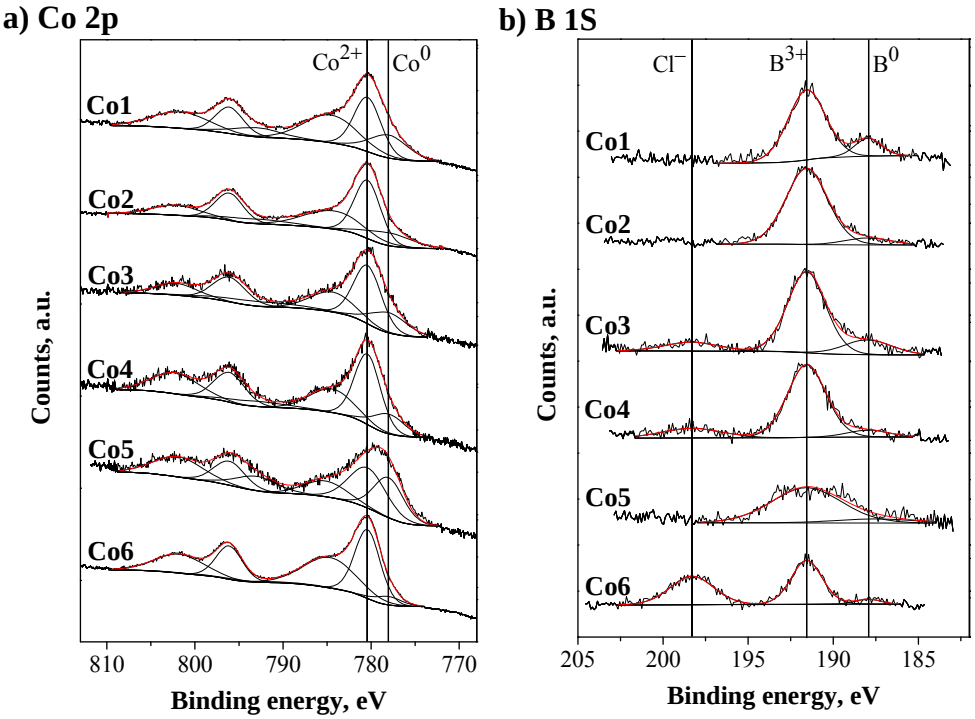


Figure 5. (a) Co 2p and (b) B 1s XPS spectra of **Co1-6** NPs.

Table 1. Percentage of Co and B species in colloidal NPs from XPS spectra decomposition.[a]

		Co 2p		B 1s		Co/B[b]
Catalyst	Polymer	Co^0	Co^{2+}	B^0	B^{3+}	
Co1	1	37	63	15	85	1.4
Co2	2	28	72	9	91	1.0
Co3	3	31	69	19	81	0.3
Co4	4	25	75	9	91	0.5
Co5	5	67	33	12	88	1.0
Co6	6	6	94	8	92	1.1

[a] Percentages corresponding to the Co $2p_{3/2}$ and B 1s spin orbit peaks.
[b] mole ratio

The large content in high valent cobalt in several of the samples suggests the presence of important amounts of cobalt oxide at the surface, in agreement with Raman spectroscopy measurements (Supporting Information). It was therefore concluded that the nature of the polymeric stabilizer used during the synthesis affects the oxidation state of the Co atoms at the surface of the final CoNPs. The differences in the reduction degree of the CoNPs could derive from the capacity of the stabilizing agent to protect the NPs against surface passivation, as previously reported.[31-33] For instance, Schmidt and co-workers reported that the oxidation rate of cobalt nanoparticles stabilized by carboxylic acid-telechelic polystyrene (Co@PS) was lower than those stabilized by polycaprolactone (Co@PCL).[32] According to the authors, this result was explained by the difference in molecular oxygen diffusion resulting from the polarity and oxygen affinity of these polymers.

Since B-doping frequently occurs during the synthesis of cobalt nanoparticles prepared by $NaBH_4$ reduction,[29, 34, 35] analysis of the oxidation state of boron species present at the NPs surface was also performed by XPS. According to Figure 5, the B 1s XPS spectra of the **Co1-6** evidenced the presence of two bands at 187.97 and 191.5 eV which evidenced the presence of cobalt borides (Co_xB) and boron oxide or borate species, respectively.[36, 37] Deconvolution of the B 1s XPS revealed the abundance of high valent boron species (> 80%, 191.5 eV, Table 1). A third band was detected at higher binding energy (198.3 eV) in **Co3**, **Co4** and more importantly in **Co6**, which corresponded to Cl 2p. The relatively larger content of chloride detected in **Co6** (1 atom% respect to the sum of all the surface species), is comprehensible considering that the stabilizer used to prepare this NPs (**Polymer6**) had chloride as counterion of the quaternary ammonium groups (Figure 1). The molar ratio between the cobalt and boron at the NPs surface (Table 1) revealed that the series of CoNPs can be divided in two groups: those with relatively large cobalt content at the surface vs. boron, with Co/B ratios above 1 (**Co1**, **Co2**, **Co5** and **Co6**), and those in which in contrast, the boron content is superior to that of cobalt (**Co3** and **Co4**). It is concluded that the boron doping at the metal surface highly depends on the polymeric stabilizer used during the synthesis of the CoNPs.

Quantification of the content in cobalt and boron in the bulk of **Co1-6** was performed by ICP (Supporting Information). The Co/B ratio for the series of CoNPs was in the range of 2.0-6.4. The maximal and minimal values in Co/B atom ratio corresponded to **Co4** (6.4) and **Co6** (2.0) respectively, while the other NPs exhibited values of *ca.* 2.6. Several studies have described the dependence of the final composition of the cobalt nanoparticles[38] and cobalt amorphous borides[34] on the reaction temperature,[39] the pH, and the borohydride concentration or borohydride/cobalt ratio.[39-42] To the best of our knowledge, this is the first study revealing the influence of the polymer stabilizer on the final composition of boron doped cobalt nanoparticles synthesized by $NaBH_4$ reduction.

The thermal stability of the NPs **Co1-6** and their corresponding polymeric stabilizers was examined by thermogravimetric analysis. The thermograms of **Co1-6** (Supporting Information) exhibited a first weight loss in the region of 90-120 ºC attributed to the loss of adsorbed solvent, followed by one or several weight losses at higher temperature (>150 ºC) corresponding to the loss of the polymeric stabilizer. According to the TGA data summarized in Table 2, important polymer amounts were detected in **Co3**, **Co4**, **Co2** (26, 12 and 7 wt%) while negligible quantities of polymer were detected in **Co1**, **Co6** and **Co5** (3, 2 and 0 wt% respectively). This clearly indicated that depending on the polymer used, distinct amounts of such stabilizer can remain at the NP surface.

Table 2. Weight losses observed by TGA for **Co1-6** NPs.

		Weight losses, wt %	
Entry	NPs	Solvent[a]	Polymer[b]
1	**Co1**	-4	-3
2	**Co2**	-8	-7
3	**Co3**	-8	-26
4	**Co4**	-3	-12
5	**Co5**	-1	0
6	**Co6**	-3	-2

[a] Weight losses at T < 120ºC. [b] Weight losses at T > 150ºC.

Analysis of the NPs by FTIR confirmed the presence of the polymer stabilizer in **Co3** and **Co4**, in agreement with TGA analysis (Supporting Information). Interestingly, the two CoNPs exhibiting relevant polymer content (**Co3** and **Co4**) were synthesized using the polymers with the lowest molecular weight of the series (10000 for **Polymer3** and 9500 g mol^{-1} for **Polymer4**) while no polymer at all was detected for **Co5** which are the NPs prepared by the polymer of the highest molecular weight (216000 g mol^{-1} for **Polymer5**). These results indicate a trend between the polymer content at the surface of the CoNPS and the molecular weight of the polymer used in their synthesis. Interestingly, Golas *et al*. described that short polymeric chains act as efficient stabilizers, resulting in well dispersed and stable metal colloids.[43]

To summarize, a series CoNPs of *ca.* 2.6 nm stabilized by polymeric stabilizers were prepared in water by chemical reduction using $NaBH_4$. Analysis of these NPs by several

techniques (HR-TEM, XRD, ICP, XPS and FTIR) revealed that the polymer stabilizer has important impact on the resulting NPs since in this study, effects on the fine structure, the composition, the reduction degree and the polymer content at the metal surface of the CoNPs were evidenced.

3.2. Characterization of TiO_2 supported catalysts (Co1-6/TiO_2)

Immobilization of **Co1-Co6** NPs on TiO_2 was carried out by direct addition of the CoNPs previously dispersed in hexane over a stirred suspension of TiO_2 in the same solvent. The amounts of NPs and TiO_2 were adjusted to obtain a cobalt loading of 10 wt% approx. Subsequently, sonication of the obtained material was performed to ensure a good dispersion of the NPs onto the support. According to the TEM micrographs of the supported catalysts, (**Co1-6/TiO_2**, Figure 6), all the CoNPs resulted well dispersed onto the TiO_2 crystals. Importantly, the particle size of the nanoclusters remained unchanged after the immobilization process.

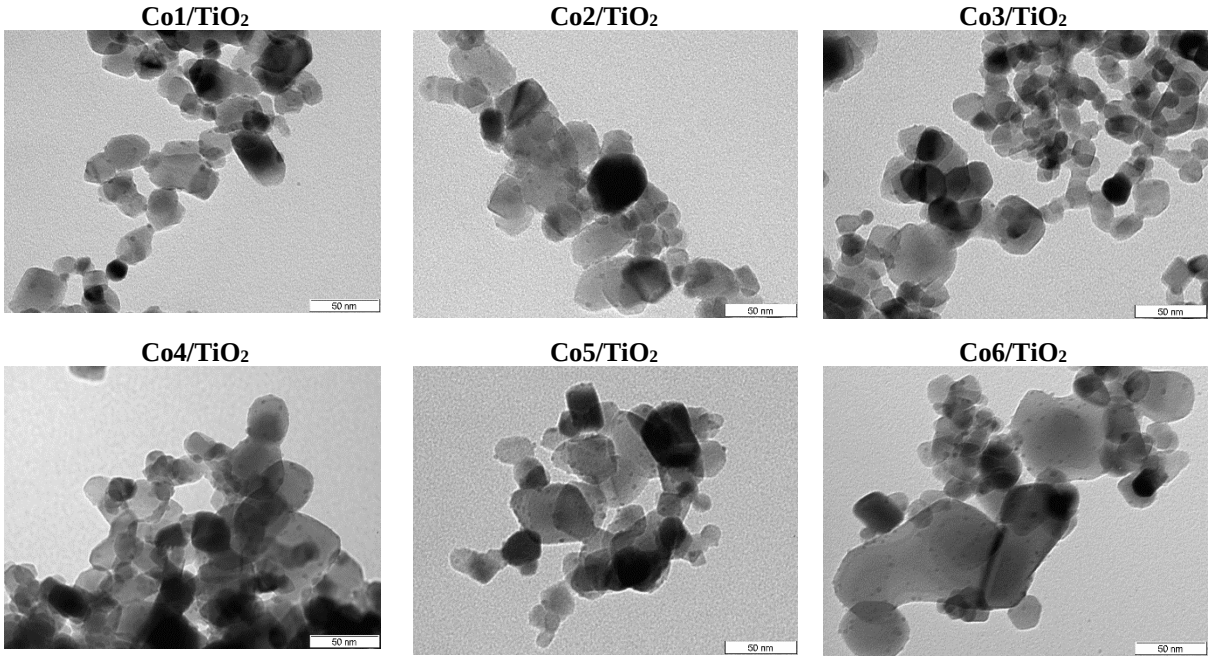


Figure 6. TEM micrographs of **Co1-6/TiO_2** catalysts.

Surface analysis of the supported catalysts was performed by XPS. Despite the low signal to noise ratio observed due to the low cobalt loading in the catalysts (*ca.* 10 wt%), deconvolution of the Co $2p_{3/2}$ spin orbit peaks confirmed that the metallic cobalt contents determined for the colloidal NPs remained similar in the supported catalysts (Supporting Information). Analysis by XRD of these materials evidenced the predominance of anatase crystalline phase over rutile phase (85 vs. 15%); however, the characteristic band of the CoNPs at 45º was overlapped by one of the rutile signals.

The reducibility of the supported catalysts **Co1-6/TiO_2** was analyzed by temperature programmed reduction (TPR). Due to the partial reduction of the CoNPs during their synthesis (intrinsic of the reduction methodology used), low signals were observed during the analysis of the fresh catalysts. For this reason, and in order to prevent metal-support reactions (frequently occurring at high temperature) a soft passivation process was performed for all the catalysts prior to TPR analysis (100 ºC, 30 min under air). As displayed in Figure 7, at least two reduction bands were observed in their TPR profile at *ca.* 300-450 and 450-600 ºC. These regions corresponding to the reduction of Co_3O_4 to CoO and of CoO to Co metal respectively.[44] It is noteworthy that the shift of the reduction temperature to higher values, when compared with typical Co/TiO_2 catalysts,[45] is explained by the presence of boron, as previously reported by Saeys and co-workers.[37] The TPR profiles of **Co1-2/TiO_2** catalysts resulted quite similar with a broad band of low intensity in the region between 300-450 ºC, followed by a sharp band at 500 ºC. This suggests that the reducibility of the catalysts prepared using **Polymers 1** and **2** is comparable, in agreement with the structural similitude of both stabilizers (Figure 1). In the case of **Co3/TiO_2**, a broad band over the region of 350-580 ºC, indicated the poor reducibility of this catalyst. The important amounts of stabilizer detected in **Co3** according to TGA (26 wt%, Table 2, entry 3) in conjunction with the large residue that **Polymer3** leaves at the metal surface after thermal decomposition (30-40 wt% of residue at 400 ºC, Supporting Information), could be the responsible for the extended reduction temperature for this catalyst. In agreement with this hypothesis, the consumption of H_2 at 450 ºC coincides with the main weight loss of **Polymer3**, thus indicating that the presence of this polymer could retard the reduction until the polymer is removed from the NP surface. In contrast, a single band with a maximum at 405 ºC was observed for **Co4/TiO_2**, and no H_2 absorption was detected for temperatures higher than 480 ºC. Finally, the TPR profile of **Co5/TiO_2** included two defined bands at 460 and 540 ºC while that of **Co6/TiO_2** was similar but the former band was less intense.

In conclusion, large differences in reducibility were observed for the series of supported catalysts **Co1-6/TiO_2**. This result clearly shows the influence of the polymeric stabilizer on the properties of the resulting NPs.

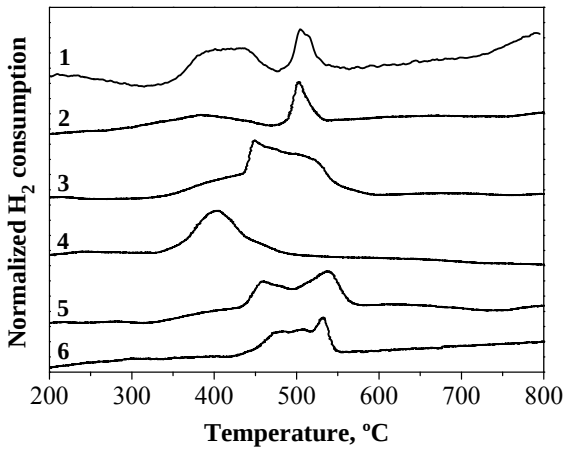


Figure 7. H_2-TPR profiles of **Co1-6/TiO_2** catalysts (1-6 respectively)**.**

N_2 physisorption analyses were also carried out on fresh catalysts. The BET areas of the series of catalysts **Co1-6/TiO_2** ranged between 42 and 56 m^2, values which are similar to that measured for TiO_2 itself (43 m^2). ICP analysis of the supported catalysts confirmed the exact cobalt loadings which ranged between 6.2-10.6 wt%.

To summarize, the supported catalysts **Co1-6/TiO_2** were prepared by simple impregnation of the corresponding colloidal NPs **Co1-6** onto TiO_2 crystals. Analyses of the supported catalysts by TEM and XPS confirmed that the particle size and the reduction degree of the CoNPs remained unchanged after immobilization of the CoNPs onto the solid support. Finally, the reducibility of the series of catalysts proved to be largely affected by the polymer stabilizer used during their synthesis.

3.3. Fischer-Tropsch catalytic experiments

Fischer-Tropsch catalytic experiments were performed using the TiO_2 supported catalysts (**Co1-6/TiO_2**) in micro fixed bed reactors. Since the catalysts had not exactly the same cobalt content, cobalt time yields were used instead of CO conversions to represent the catalytic activity. The cobalt time yields and product selectivity obtained at 240 ºC after 46 h of reaction are displayed in Table 3.

Strong differences in the cobalt time yield were observed as a function of the polymeric stabilizer used during the synthesis of the CoNPs. The series of catalysts exhibited the following order of activities at 46 h of reaction: **Co2/TiO_2** > **Co5/TiO_2** > **Co1/TiO_2** > **Co6/TiO_2** > **Co4/TiO_2** ~ **Co3/TiO_2** (Table 3).

Table 3. Fischer-Tropsch synthesis in fixed bed reactor using TiO_2 supported CoNPs[a]

E.	Catalyst	Polymer	Cobalt time yield[b]	Selectivity, Wt%					α
				CO_2	CH_4	C_{2-4}	C_{5-12}	C_{12+}	
1	**Co1/TiO₂**	1	5.27	0.0	10.5	17.4	19.0	53.0	0.76
2	**Co2/TiO₂**	2	11.76	0.3	13.1	16.0	25.9	44.7	0.81
3	**Co3/TiO₂**	3	0	0	0	0	0	0	0
4	**Co4/TiO₂**	4	0.04	0	0	0	0	0	0.88
5	**Co5/TiO₂**	5	8.62	0.0	10.5	17.7	18.6	53.2	0.73
6	**Co6/TiO₂**	6	3.20	0.0	13.6	18.2	22.9	45.3	0.81

[a] Conditions: Catalyst loading, 7-10 wt%, 20 bar $H_2/CO/N_2$ (2:1:0.15), 5.62 ml/min, 240 ºC; [b] metal time yield = mol of CO converted per mol of Co, per unit of time (46 h).

It should be noted that due to the low activity of the catalyst **Co3-4/TiO₂**, some of the products could not be quantified. Concerning the selectivity of the active catalysts (**Co1,2,5,6/TiO₂**), similar hydrocarbon fractions were obtained in all cases (10-13% CH_4, 16-18% C_{2-4}, 18-25% C_{5-12} and 44-53% C_{5+}; Table 3. and Figure 8). It is noteworthy that the production of CO_2 was negligible under the present catalytic conditions. For the particular case of **Co2/TiO₂,** slightly higher selectivity for the gasoline fraction (26 wt%, C_5-C_{12}) was observed in comparison to the other catalysts (18-23 wt%).

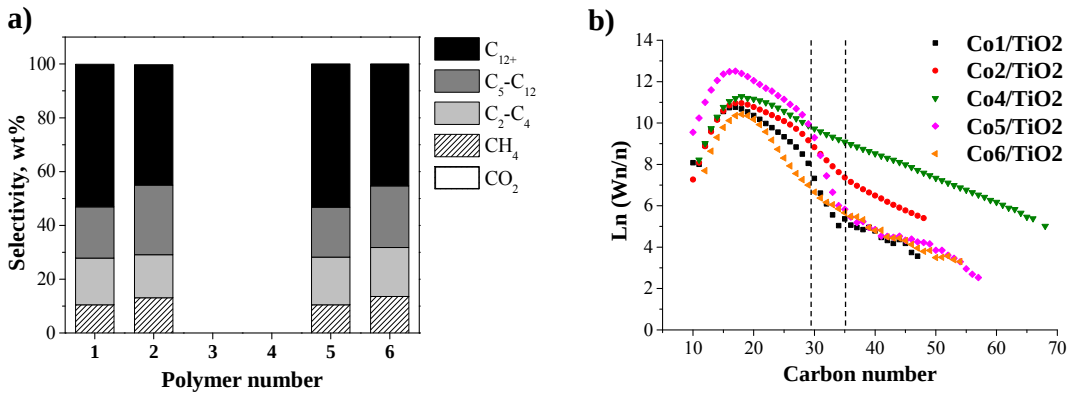


Figure 8. (a) Product selectivity in FTS as a function of the polymeric stabilizer and **(b)** ASF distributions of **Co1-6/TiO₂**. Conditions: Catalyst loading = 7-10 wt%, 20 bar $H_2/CO/N_2$ (2:1:0.15), 5.62 ml/min, 240 ºC.

Concerning the chain growth probability, the catalysts exhibited α values between 0.73-0.81. The lowest α value was registered for **Co5/TiO₂** (0.73) prepared from **Polymer5**. According to the ASF distributions displayed in Figure 8, it is noteworthy that catalysts **Co1/TiO₂** and **Co5/TiO₂** clearly presented an inflexion in the distribution near C_{30} after which the product fractions notably decreased. This inflexion seems to also appear in **Co2/TiO₂** but in a less pronounced manner. In contrast, the hydrocarbons produced by **Co6/TiO₂** positively deviated from typical ASF distributions, which means that the alpha value increases with the

increase of the carbon number. Although the activity of **Co4/TiO$_2$** was negligible, the accumulation of product during 46h of reaction allowed the analysis of the wax fraction. In this case, a typical ASF distribution was observed, resulting in a chain growth factor of 0.88, which is the highest α value of the series.

The evolution of the cobalt time yield of the catalysts during time is displayed in Figure 9. Among the active catalysts it can be noticed in **Co2/TiO$_2$**, **Co5/TiO$_2$** and **Co6/TiO$_2$** a significant decrease of activity during the first 10-20 h of reaction, before the catalysts reached the steady state. In the case of **Co1/TiO$_2$**, a less pronounced decrease in activity was observed during the first hours of reaction.

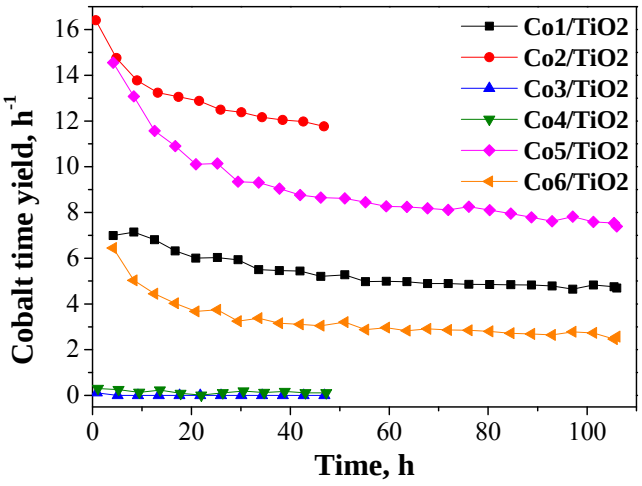


Figure 9. Evolution of cobalt time yield during time in FT experiments. Conditions: 7-10 wt% Co/TiO$_2$, 20 bar H$_2$/CO/N$_2$ (2:1:0.15), 5.62 ml/min, 240 ºC.

Deactivation rates were calculated for the series of tested catalysts computing the time yields at 2h and 46h (Supporting Information). Fast deactivation of **Co5/TiO$_2$** and **Co6/TiO$_2$** was observed during the first 20h of reaction (-44 and -52 % after 46 h respectively). A similar deactivation profile, although less pronounced, was registered for **Co2/TiO$_2$** (-26% after 46h). Other catalysts such as **Co1/TiO$_2$** presented relatively stable time yields without a marked deactivation during the initial period of the reaction.

It can therefore be concluded that the polymer used to stabilize the CoNPs strongly affect not only the activity but also the stability of the supported catalysts in the FTS. From the tested catalysts, **Co2/TiO$_2$** resulted to be the most active of series, while **Co3-4/TiO$_2$** were barely active. In addition, similar selectivities were obtained for the active catalysts with ASF distributions exhibiting an inflexion near C_{30}.

The performance in FTS of the series of catalysts was rationalized considering the properties of the supported catalysts such as the cobalt reducibility, and other parameters

intrinsic to the colloidal NPs such as the polymer and boron content and the reduction degree at the surface of the CoNPs.

On one hand, the lack of activity observed for catalysts **Co3-4/TiO$_2$** is explained by the relatively large amount of the polymeric stabilizer determined by TGA in the colloidal NPs (26 and 12 wt% respectively, Table 2). This hypothesis is based in the fact that the remaining polymer at the metal surface could block active sites of the NPs thus affecting negatively the catalyst performance.[7, 46] The high boron content at the surface of these NPs can also explain the lack of activity for these catalysts (Table 1).[47]

On the other hand, the performance of the active catalysts (**Co1,2,5,6/TiO$_2$**) can be mainly correlated with the reducibility or the reduction degree of the colloidal NPs since it is indicative of the metallic cobalt content at the beginning of the catalysis. The correlation between the catalytic performance and the interval of reduction temperatures for the supported catalysts (extracted from TPR analysis) is depicted in Figure 10. Indeed, the high activity observed for **Co2/TiO$_2$** agrees with the good reducibility of this catalyst considering the relatively low temperature at which this starts to reduce (280 ºC, the lowest of series). In contrast, the high reduction temperature required for **Co6/TiO$_2$** (420-550 ºC) which is above the activation temperature explains its low activity compared to the other catalysts. Additionally, the performance of this catalyst could also be affected by the presence of chloride, which is a known poison in FT.[48] Finally, the superior activity of **Co5/TiO$_2$** compared to that of **Co1/TiO$_2$**, despite of their similar reduction temperature (320-570 ºC vs. 320-560 ºC) is rationalized in terms of the metallic cobalt content at the surface of the colloidal NPs which is higher for **Co5** than for **Co1** according to XPS (67 vs. 37 %, Table 1). Indeed, the initial metallic cobalt content will assist the reduction during the activation process, making **Co5/TiO$_2$** more reducible than **Co1/TiO$_2$**, as reported by Martens et al. for Co/TiO$_2$ supported catalysts.[45]

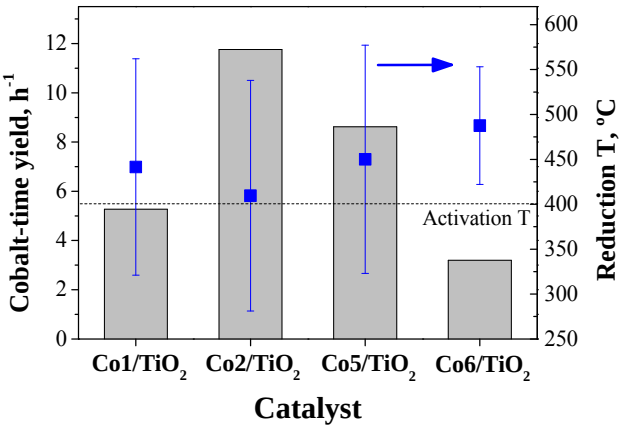


Figure 10. Correlation between the activity and the interval of reduction temperatures (measured by TPR) of the supported catalysts **Co1,2,5,6/TiO$_2$**.

To conclude, the catalytic performance of the TiO_2 supported catalysts in FTS was deeply affected by parameters such as the reducibility of the catalysts, the polymer/boron content and the initial metallic cobalt at the surface of colloidal CoNPs, which in turn were shown to be correlated with the properties of the polymeric stabilizer used during the preparation of the nanoparticles.

4. Conclusions

A series of CoNPs of *ca.* 2.6 nm stabilized by polymers were synthesized in water using $NaBH_4$ as reducing agent. Supported catalysts were also prepared by simple impregnation of the colloidal NPs onto TiO_2. This approach allowed the fine modulation of the particle size and permitted detailed characterization of the cobalt nanoparticles before of their immobilization on the solid support. Notable differences in fine structure, reduction degree, composition and polymer content were identified for the colloidal NPs as a function of the polymeric stabilizer. Analysis of the TiO_2 supported catalysts confirmed that the particle size of the CoNPs and the trend in reduction degree observed in the colloidal NPs remained unaltered after immobilisation. The reducibility of the catalysts resulted to be deeply influenced by the polymeric stabilizer.

The catalytic performance of the supported catalysts resulted also deeply dependent on the nature of the polymeric stabilizer. Parameters such as the catalyst reducibility, the amount of the polymeric stabilizer remaining at the metal surface and the metallic cobalt content at the nanoparticle surface were considered to rationalize the performance of these catalysts.

Acknowledgements

The authors are grateful to Total S.A., the Spanish Ministerio de Economía y Competitividad (CTQ2013-43438-R, and *Ramon y Cajal* fellowship to C. Godard) and the Generalitat de Catalunya (2014SGR670) for financial support. We also thank the Prof. Andrei Khodakov for his contribution concerning the Fischer-Tropsch experiments with supported catalysts.

References

[1] A. Steynberg, Fischer-Tropsch Technology, in: A. Steynberg, M. Dry (Eds.) Fischer-Tropsch Technology. Studies in Surface Science and Catalysis, Elsevier, 152, Amsterdam, The Netherlands, 2006, pp. 1-3.
[2] L.P. Dancuart, A. Steynberg, in: B.H. Davis, M.L. Occelli (Eds.) Fischer-Tropsch synthesis, catalysts and catalysis, Elsevier, Eastbourne, UK, 2007, pp. 379-381.
[3] Q. Zhang, J. Kang, Y. Wang, ChemCatChem, 2 (2010) 1030-1058.
[4] V.R. Calderone, N.R. Shiju, D. Curulla-Ferré, S. Chambrey, A. Khodakov, A. Rose, J. Thiessen, A. Jess, G. Rothenberg, Angew. Chem. Int. Ed., 52 (2013) 4397-4401.
[5] A. Gual, C. Godard, S. Castillón, D. Curulla-Ferré, C. Claver, Catal. Today, 183 (2012) 154-171.
[6] L.S. Ott, R.G. Finke, Coord. Chem. Rev., 251 (2007) 1075-1100.
[7] X.Y. Quek, R. Pestman, R.A. van Santen, E.J.M. Hensen, ChemCatChem, 5 (2013) 3148-3155.

[8] J. Llop Castelbou, E. Bresó-Femenia, P. Blondeau, B. Chaudret, S. Castillón, C. Claver, C. Godard, ChemCatChem, 6 (2014) 3160-3168
[9] X. Wang, P. Sonström, D. Arndt, J. Stöver, V. Zielasek, H. Borchert, K. Thiel, K. Al-Shamery, M. Bäumer, J. Catal., 278 (2011) 143-152.
[10] H.R. Choi, H. Woo, S. Jang, J.Y. Cheon, C. Kim, J. Park, K.H. Park, S.H. Joo, ChemCatChem, 4 (2012) 1587-1594.
[11] L.M. Martínez-Prieto, S. Carenco, C.H. Wu, E. Bonnefille, S. Axnanda, Z. Liu, P.F. Fazzini, K. Philippot, M. Salmeron, B. Chaudret, ACS Catal., 4 (2014) 3160-3168.
[12] L. Liu, G. Sun, C. Wang, J. Yang, C. Xiao, H. Wang, D. Ma, Y. Kou, Catal. Today, 183 (2012) 136-142.
[13] X.B. Fan, Z.Y. Tao, C.X. Xiao, F. Liu, Y. Kou, Green Chem., 12 (2010) 795-797.
[14] H. Wang, W. Zhou, J.X. Liu, R. Si, G. Sun, M.Q. Zhong, H.Y. Su, H.B. Zhao, J.A. Rodriguez, S.J. Pennycook, J.C. Idrobo, W.X. Li, Y. Kou, D. Ma, J. Am. Chem. Soc., 135 (2013) 4149-4158.
[15] H. Wang, Y. Kou, Chin. J. Catal., 34 (2013) 1914-1925.
[16] A. Meffre, B. Mehdaoui, V. Connord, J. Carrey, P.F. Fazzini, S. Lachaize, M. Respaud, B. Chaudret, Nano Lett., 15 (2015) 3241-3248.
[17] M. Scariot, D.O. Silva, J.D. Scholten, G. Machado, S.R. Teixeira, M.A. Novak, G. Ebeling, J. Dupont, Angew. Chem. Int. Ed., 47 (2008) 9075-9078.
[18] D.O. Silva, J.D. Scholten, M.A. Gelesky, S.R. Teixeira, A.C.B. Dos Santos, E.F. Souza-Aguiar, J. Dupont, ChemSusChem, 1 (2008) 291-294.
[19] http://avantium.com/catalysis/R-D-solutions/systems/Flowrence.html.
[20] Y. Chen, K.Y. Liew, J. Li, Appl. Surf. Sci., 255 (2009) 4039-4044.
[21] K.S. Chou, Y.C. Chang, L.H. Chiu, Ind. Eng. Chem. Res., 51 (2012) 4905-4910.
[22] R. Seoudi, A. Shabaka, Z.A. El Sayed, B. Anis, Physica E, 44 (2011) 440-447.
[23] L.T. Lu, L.D. Tung, I. Robinson, D. Ung, B. Tan, J. Long, A.I. Cooper, D.G. Fernig, N.T.K. Thanh, J. Mater. Chem., 18 (2008) 2453-2458.
[24] R.G. Shimmin, A.B. Schoch, P.V. Braun, Langmuir, 20 (2004) 5613-5620.
[25] J.A. Delgado, C. Claver, S. Castillón, D. Curulla-Ferré, C. Godard, ACS Catal., (2015) 4568-4578.
[26] J.A. Delgado, S. Castillón, D. Curulla-Ferré, C. Claver, C. Godard, Catal. Commun., 71 (2015) 88-92.
[27] J. Garcia-Torres, E. Vallés, E. Gómez, J. Nanopart. Res., 12 (2010) 2189-2199.
[28] C. Petit, Z.L. Wang, M.P. Pileni, J. Phys. Chem. B, 109 (2005) 15309-15316.
[29] G.N. Glavee, K.J. Klabunde, C.M. Sorensen, G.C. Hadjipanayis, Langmuir, 9 (1993) 162-169.
[30] A.Y. Khodakov, W. Chu, P. Fongarland, Chem. Rev., 107 (2007) 1692-1744.
[31] N. Doan, K. Kontturi, C. Johans, J. Colloid Interface Sci., 350 (2010) 126-131.
[32] C. Dobbrow, A.M. Schmidt, Beilstein J. Nanotechnol., 3 (2012) 75-81.
[33] X.H. Zhang, K.M. Ho, A.H. Wu, K.H. Wong, P. Li, Langmuir, 26 (2010) 6009-6014.
[34] S. Carenco, D. Portehault, C. Boissière, N. Mézailles, C. Sanchez, Chem. Rev., 113 (2013) 7981-8065.
[35] G.N. Glavee, K.J. Klabunde, C.M. Sorensen, G.C. Hadjipanayis, Inorg. Chem., 32 (1993) 474-477.
[36] G.M. Arzac, T.C. Rojas, A. Fernández, ChemCatChem, 3 (2011) 1305-1313.
[37] K.F. Tan, J. Chang, A. Borgna, M. Saeys, J. Catal., 280 (2011) 50-59.
[38] U.B. Demirci, P. Miele, Phys. Chem. Chem. Phys., 16 (2014) 6872-6885.
[39] I. Dragieva, G. Gavrilov, D. Buchkov, M. Slavcheva, J. Less Common Met., 67 (1979) 375-379.
[40] S.r. Linderoth, S. Mo/rup, J. Appl. Phys., 69 (1991) 5256-5261.
[41] Y. Wang, H. Wu, Q. Zhang, Q. Tang, Micropor. Mesopor. Mat., 86 (2005) 38-49.
[42] L. Yiping, G.C. Hadjipanayis, C.M. Sorensen, K.J. Klabunde, J. Magn. Magn. Mater., 79 (1989) 321-326.
[43] P.L. Golas, S. Louie, G.V. Lowry, K. Matyjaszewski, R.D. Tilton, Langmuir, 26 (2010) 16890-16900.
[44] A.Y. Khodakov, W. Chu, P. Fongarland, Chem. Rev., 107 (2007) 1692-1744.
[45] J.H.A. Martens, H.F.J. Van 't Blik, R. Prins, J. Catal., 97 (1986) 200-209.
[46] A. Yarulin, I. Yuranov, F. Cárdenas-Lizana, D.T.L. Alexander, L. Kiwi-Minsker, App. Catal. A-Gen, 478 (2014) 186-193.
[47] J. Li, N.J. Coville, App. Catal. A-Gen, 181 (1999) 201-208.
[48] C.H. Bartholomew, in: L. Guczi (Eds.), Studies in Surface Science and Catalysis, Elsevier, 1991, pp. 158-224.